

# Deep Multi-Scale U-Net Architecture and Noise-Robust Training Strategies for Histopathological Image Segmentation

Nikhil Cherian Kurian<sup>\*1</sup>, Amit Lohan<sup>\*1</sup>, Gregory Verghese<sup>2,3,4</sup>, Nimish Dharamshi<sup>1</sup>, Swati Meena<sup>1</sup>, Mengyuan Li<sup>2,3</sup>, Fangfang Liu<sup>2,5</sup>, Cheryl Gillet<sup>6</sup>, Swapnil Rane<sup>7</sup>, Anita Grigoriadis<sup>2,3,4</sup>, and Amit Sethi<sup>1</sup>

<sup>1</sup> Department of Electrical Engineering, Indian Institute of Technology Bombay  
Mumbai, India

<sup>2</sup> Cancer Bioinformatics, School of Cancer & Pharmaceutical Sciences, Faculty of Life Sciences and Medicine, King's College London London, UK.

<sup>3</sup> School of Cancer & Pharmaceutical Sciences, King's College London Faculty of Life Sciences and Medicine, London, UK.

<sup>4</sup> Breast Cancer Now Unit, School of Cancer and Pharmaceutical Sciences, King's College London, London, UK.

<sup>5</sup> Department of Breast Pathology and Research Laboratory, Key Laboratory of Breast Cancer Prevention and Therapy (Ministry of Education), National Clinical Research Center for Cancer, Tianjin Medical University Cancer Institute and Hospital, Tianjin, China.

<sup>6</sup> CRUK King's Health Partners Centre, King's College London, Innovation Hub, Cancer Centre at Guy's Hospital, Great Maze Pond, London, UK.

<sup>7</sup> Dept. of Pathology, Tata Memorial Centre-Tata Memorial Hospital, HBNI, Mumbai, India

**Abstract.** Although the U-Net architecture has been extensively used for segmentation of medical images, we address two of its shortcomings in this work. Firstly, the accuracy of vanilla U-Net degrades when the target regions for segmentation exhibit significant variations in shape and size. Even though the U-Net already possesses some capability to analyze features at various scales, we propose to explicitly add multi-scale feature maps in each convolutional module of the U-Net encoder to improve segmentation of histology images. Secondly, the accuracy of a U-Net model also suffers when the annotations for supervised learning are noisy or incomplete. This can happen due to the inherent difficulty for a human expert to identify and delineate all instances of specific pathology very precisely and accurately. We address this challenge by introducing auxiliary confidence maps that emphasize less on the boundaries of the given target regions. Further, we utilize the bootstrapping properties of the deep network to address the missing annotation problem intelligently. In our experiments on a private dataset of breast cancer lymph nodes, where the primary task was to segment germinal centres and sinus histiocytosis, we observed substantial improvement over a U-Net baseline based on the two proposed augmentations.

---

\* Equal contribution

## 1 Introduction

In pathology, hematoxylin and eosin (H&E) stained histopathological whole-slide images (WSIs) are sources of rich diagnostic information[1,2]. Various segmented regions of a WSI can give biomarker information, such as areas in various histologically distinct regions and their ratios. Deep learning has become a framework of choice for automating segmentation with high accuracy, provided a large dataset of annotated images is available for training[3]. Within deep learning, architectures inspired from the U-Net have been widely adopted due to their unique ability to both gather evidence for semantic segmentation from somewhat large receptive fields, and yet be able to produce fine-grained and precise boundaries [4]. However, U-Net has been shown to perform poorly when the target regions exhibits large variations in their shape and scale that is common in histology [5,6]. This challenge is common in our target problem, where we want to segment germinal centers (GC) or sinus-histiocytosis in breast cancer lymph node slides. In this work we present Multi-Scale U-Net (MS U-Net), a lightweight architecture that performs effective segmentation of histology images by introducing explicit multi-scale feature extraction in the U-Net encoder. We compare the performance of our architecture to a U-Net baseline. To account for edge artifacts and padding issues arising when the constituent patches of WSI are segmented independently, we also propose a better loss calculation strategy for each image patch. Here we calculate the loss only on the centre cropped regions from each patch, and subsequently the segmentation mask from these regions are only utilised to stitch back and create a smooth whole slide level segmentation mask.

Furthermore, the advantage of high accuracy offered by most of the deep learning networks is realized only when a large and accurately labeled dataset is available for supervised learning [7]. For tissue region segmentation on WSIs, the large dimensions of these images and inherent continuums in lesion grades make it prohibitively difficult for a human annotator to mark exact boundaries of various tissue regions in addition to avoiding errors of totally missing some small regions from annotations. Thus, the quality of annotations provided by a human expert in these settings are often inaccurate and noisy. Such noisy supervision degrades the performance of the deep learning model, especially in case of segmentation task where the ground truth involves pixel level annotations [7]. In an endeavor to address these challenges, we explore and adapt certain robust deep learning training strategies to further improve our segmentation results on top of our proposed MS U-Net architecture. Specifically, we relax the strict imposition of cross-entropy (CE) loss at the boundary of annotations where the annotator are most uncertain, through blurred confidence maps that modulate the original CE loss. Also, we attempt to address the challenging problem of missing annotations through a bootstrapping framework, where we gather the most confident model predictions from early training iterations as auxiliary masks that can enhance model predictions in case of missing annotations.

## 2 Related Work

### 2.1 Multi-Resolution Segmentation

The most widely used architecture for medical segmentation is the U-Net model, which consists of an encoder and a decoder module each [4]. Although the pooling and up-convolution operations in a U-Net give it some ability to process information at multiple scales, in several followup works the U-Net model has been improved by explicitly incorporating multi-resolution processing capabilities. These proposed multi-resolution image analysis architectures can effectively fuse the contextual information of a tissue with its nuclear level morphologies. We give some examples next.

In [8], a multi-scale information extractor was utilised to process patches at multiple resolution at each layer of the encoder stage after passing through a convolutional layer. An alternate method was suggested in [9], where they used multiple separate encoder and decoders for patches taken from different resolution. They further concatenated these separate decoders at multiple decoder layers. The concept of multi-path training was explored in [10], where they used three separate paths for encoding features at three separate resolutions, where each path consists of dense blocks. Also each path in the model is trained individually and separately, along with an overall end to end training. An advanced architecture presented in [11] incorporates three different resolutions with use of three different expert convolutional neural networks (CNN) trained individually, the output features are then concatenated together and passed through another aggregating CNN for an end to end model training. The concatenation is done using adaptive weights where the weight for each individual expert CNN is found using another CNN.

Though these methods effectively fuse multi-resolution information for segmentation, these architectures are computationally expensive and difficult to train.

### 2.2 Learning from Noisy Annotations

Noisy annotations are almost unavoidable in certain types of medical images, especially when these have continuum of disease grades, numerous objects of varied sizes to be segmented, or low contrast or intricate boundaries between anatomical structures. This problem is more challenging when multiple annotators work on the same image. Deep learning-based medical image segmentation in the face of noisy or incomplete ground truth masks is a challenging problem gaining some attention [12,13]. In mandible CT images Yu et.al [14] studied the effect of noisy annotations in a deep learning-based segmentation. The study empirically highlighted the degradation of deep learning model performance when trained with noisy ground truth mask. Similarly, in [13], the authors explicitly show the negative impact of missing annotations in deep segmentation models for medical imaging. However, more work is needed to effectively address this problem.

### 3 Methodology

#### 3.1 Multi-Scale U-Net Architecture

The proposed architecture modifies the original encoder block of the U-Net architecture, where we introduce a downsampling block with multiple kernels for producing feature maps at different scales. The architecture of the downsampling blocks in the proposed Multi-scale U-Net (MS U-Net) model is shown in Figure 1. Though the high-level architecture is similar to that of a U-Net, but each downsampling block on the encoder side contains the modification capable of multi-scale processing. In a typical U-Net block, there are two convolutional layers and the output feature map is passed through a max-pooling layer. In the proposed multi-scale architecture, each block contains three sets of kernels in the first convolutional layer, where each set works at a different scales. That is, one set of kernels works at the resolution of input to the block, another set has a dilation and stride of two to reduce the resolution to a half, and a third set has a dilation and stride of four to reduce the resolution to a fourth of the input.

The outputs of the two sets of kernels that downscale the feature maps scaled back up to the original resolution using bilinear interpolation and concatenated with the feature maps of the first set of kernels to make a single set of feature maps. This set of feature maps is then passed to a max-pool layer before being sent to the next block where the same sequence of operations is repeated. In the decoder, blocks that have an up-convolution are then passed these extracted encoder features from corresponding level concatenated along with previous layer decoder feature maps. After the interpolation and concatenation of the two feature maps, they are passed through single convolutional layer before passing outputs to next decoder block.

#### 3.2 Augmentations

Augmenting the training data by randomly rotating the images and their segmentation maps have been found to be useful for improving the segmentation results. For whole slide images, as the training is done at the patch level and final prediction is required to be done at the whole slide image level, it is important to feed the patches without any artificial background to the network. This was done by creating  $\sqrt{2} \times \sqrt{2}$  times larger patches (1444x1444) than the actual size (1024x1024) used for training. With respect to the center of the larger patch, after randomly deciding a rotation angle, four coordinates of the rotated patch are calculated and the rotated patch is then extracted as square patch using affine transformation. This way the actual patch is created by extracting a randomly rotated patch from the center of larger patches. Along with this, horizontal and vertical flipping augmentations were carried out, as well as colour jitter with brightness, saturation, hue and contrast as 0.15.

#### 3.3 Robust Training Strategies for Noisy Annotations

The annotation procedure is quite laborious and the provided annotations are almost always inevitably noisy, especially with a large amount of incorrectly

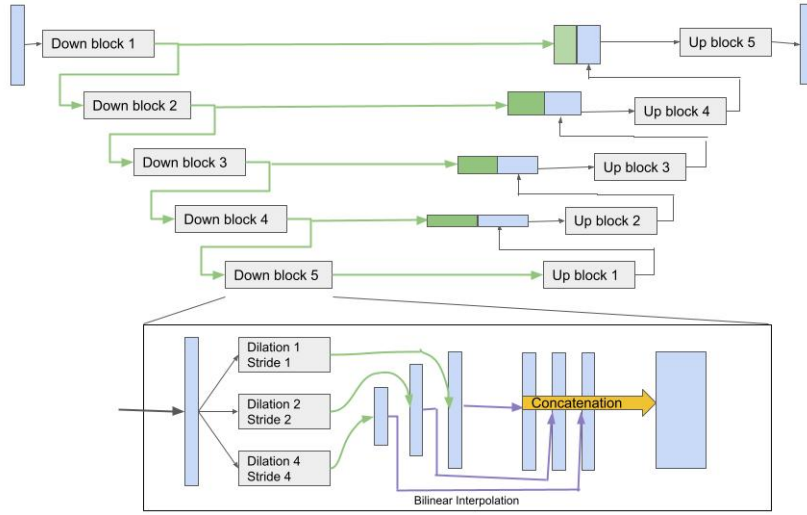


**Fig. 1.** Proposed Multi-Scale U-Net (MS U-Net) model architecture with the encoder block expanded to show the multi-scale processing of segmentation features.

marked pixels for regions such as sinus and follicle, where even pathologists may disagree on the correct label for a region of pixels. Thus, we inevitably give the neural network some wrong labels for some of the regions to learn from, and that makes it to produce poor results at the test time. Using sinus as an example, the two major problems of inaccurate boundaries and missing annotations (where some sinus region might be completely ignored by annotator), are shown in figure 3(b).

**Fuzzy Boundaries** helps deal with inaccurate boundaries of annotations. In this technique, while computing the loss for the prediction of a patch, an additional mask is computed by blurring the edges in the original segmentation mask. This blurred mask is then subtracted from the original mask and the absolute value at each location is taken. This mask is then normalized and subtracted from a mask of all 1's. This way we finally obtain a mask indicating the confidences with value 1's at the regions away from any kind of boundaries and smaller values closer to 0, near to and on the boundaries, depending on the gradient of each location. An example of fuzzy masks have been shown in 4. This mask is then multiplied with the cross entropy loss values calculated for respective locations. Finally the overall loss is averaged. This way, the values closer to boundaries contribute less to the loss calculation and the values away from boundaries contribute more. That is, we let the model decide for the locations closer to boundaries and don't force it to learn the labels marked in annotations. Weights for fuzzy boundary,  $w_{fb}$ , are given in equation 1 as,

$$w_{fb} = 1 - \text{abs}(t - g(t, k)) \quad (1)$$

where,  $g()$  is the Gaussian blurring function,  $\text{abs}()$  is the absolute function,  $t$  is normalized target mask,  $k$  is kernel size for blurring

For the blurring, if the patch is from a normal dataset, a Gaussian blurring is applied using kernel size of (21,21), and if the patch is from noisy dataset, then a Gaussian blurring of kernel size (61,61) is applied. That is, on a noisy dataset we have less trust in the boundary locations given by the annotator, hence we want it to be more fuzzy, or having lower importance in loss computation. Figure 4 (a) and (b) shows the difference between confident and noisy mask annotations fuzzy boundaries.

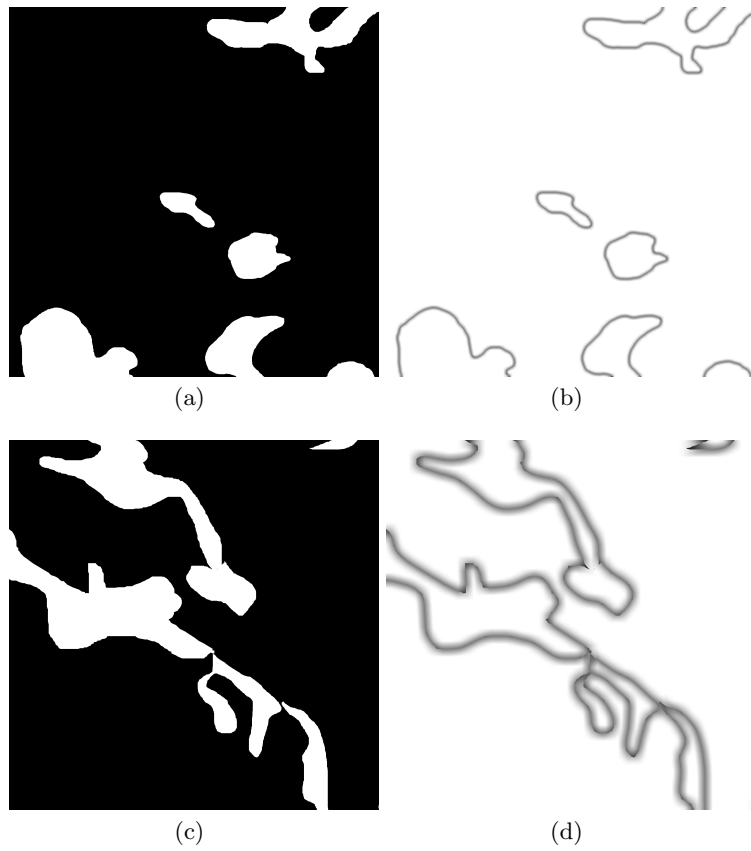


**Fig. 2.** (a) Sample image of a normal mask, (b) Illustrating fuzzy boundary on the normal mask with a kernel size of 21, (c) Sample image of a noisy mask, (d) Fuzzy boundary maps created from the noisy mask with a kernel size of 61

**Bootstrapping** deals with missing annotations by pathologists. In bootstrapping, we train the network for a few epochs, where it learns to segment regions which can clearly be said to belong to a class or not with confidence.

Then, accordingly the network modifies the weight given to different regions of the predictions of the network in loss calculation. This way, in addition to the ground truth mask used for segmentation, the prediction of network itself, which acts as an auxiliary mask, is used to compute the loss by deciding a weight map for it. The network’s prediction masks are used only after training it for  $n$  number of epochs, which is a hyperparameter. One such WSI example is shown in figure 3 where some of the existing annotations are missing, which is highlighted in the figures by a green box. Here, the model prediction correctly identifies the region with a high confidence, and hence the model prediction should be considered as an auxiliary mask.

For implementing the bootstrapping method, we compute bootstrap weight matrix  $w_{bs}$ . In our experiments, after 10 iterations, the loss function is spatially weighted by  $w_{bs}$ , given in equation 2 as,

$$w_{bs} = 2 * abs(0.5 - p) \quad (2)$$

where,  $p$  is the model prediction output after passing through a softmax layer. So,  $w_{bs}$  basically pushes those model predictions with higher confidence (prediction values close to 0 or 1) to higher magnitude and other predictions with lower confidence (prediction values close to 0.5) to lesser magnitude, and computes  $w_{bs}$ . This reduces the impact of lower confidence regions on the loss computation.

The overall weights given to the loss calculation,  $w_{total}$  is a combination of fuzzy part as well as bootstrapping part with weights  $\beta$  and  $1 - \beta$  as a hyperparameter, as given in equation 3,

$$w_{total} = \beta * w_{fb} + (1 - \beta) * w_{bs} \quad (3)$$

In our experiments, we kept the value of  $\beta$  as 0.5

### 3.4 Loss Functions

We used weighted cross entropy loss to counter the imbalance between the numbers of pixels belonging to foreground or background (approximately 1:10), by using an inverse of their ratio. For a noisy dataset, this loss is then multiplied by a confidence mask created using the fuzzy boundary and bootstrapping techniques.

We also countered the impact of missing context near the edges of the patches by using center-cropped loss calculation. That is, the loss for a pre-defined margin of a patch is discarded for training.

The weighted cross entropy loss  $l_{wce}$  is given by the equation 4 as,

$$l_{wce} = \sum (w_{bg} * p_{bg} * t_{bg} + w_{fg} * p_{fg} * t_{fg}), \quad (4)$$

where  $w_{bg}$  is the background pixels weight, and  $w_{fg}$  is the foreground pixels weight

The final loss  $l$  is given by the equation 5 as follows:

$$l = l_{wce} * w_{total} \quad (5)$$

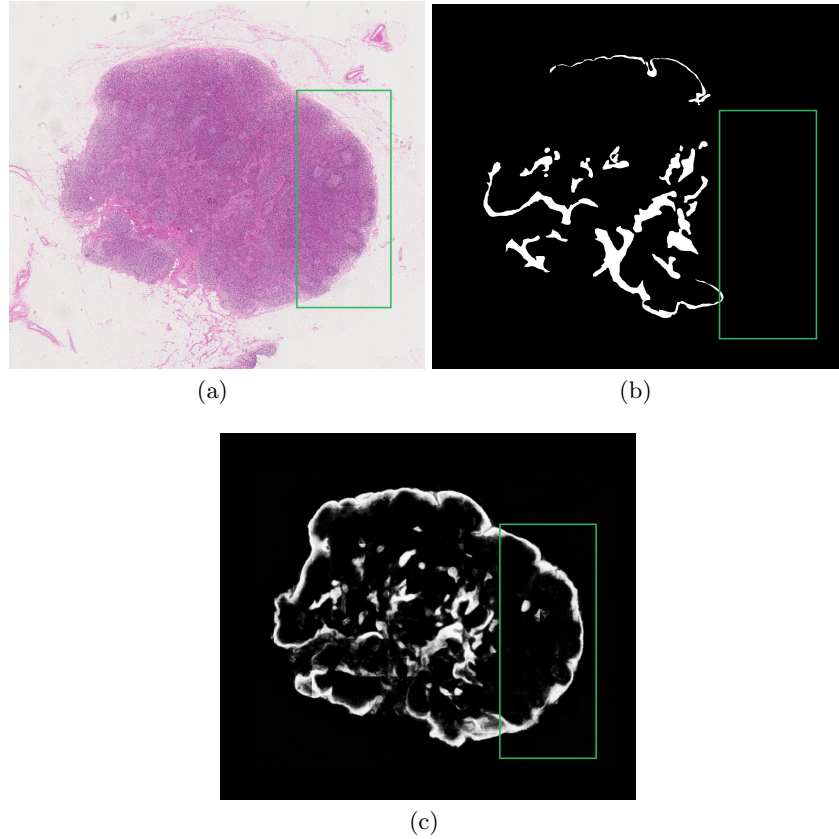


**Fig. 3.** (a)The original WSI input to the U-Net architecture, (b) The WSI mask with missing annotations of certain sinus regions as shown in the green box (c) The mask predicted by our model in its bootstrapping period indicating the presence of missing region

### 3.5 Evaluation Metrics

For segmentation, a large WSI is often divided into constituent patches that are individually segmented by a deep learning model. The segmentation mask from these patches are then stitched back to finally create a WSI level segmentation mask. For our analysis, we used intersection over union (IoU) score as the evaluation metric at the WSI level. The value of IoU score ranges in between 0 – 1, and a larger value is desirable.

Along with the IoU score, for qualitative evaluation we also overlaid images prediction with input WSI image and its ground truth. For overlaying ground truth with prediction, we represent the true positive region, false positive region and false negative region with green, red and blue regions, respectively. This is overlaid over the input WSI image, as shown in an example in Figure4 (c).



### 3.6 Data Preparation

The dataset comprises of whole slide images (WSIs) of lymph node regions, obtained from a private repository of breast cancer WSIs of lymph node data collected from Guy’s hospital, London. Annotations were performed independently by two pathologists. The pixel-wise annotations were carefully created to identify and mark all regions of sinus and germinal centre (GC) for 50 WSIs.

There are two experiments mentioned below, one focusing on comparison of training results of plain U-Net with MS U-Net model, and another focusing on comparison of training results obtained from different robust methods like fuzzy boundary and bootstrapping.

For the first experiment, 20 WSIs were used for training, 8 WSIs were used for validation, and the 5 WSIs with extensive and most carefully annotated images were used for testing. A total of 11,000 image patches were extracted in the preprocessing stages of training the segmentation model. All experiments are conducted on level 2 WSIs, i.e. at 10x resolution. A patch-wise training approach was followed, for which there was a 50% overlapping region between adjacent extracted patches from the WSIs. Patches of 1024x1024 size were extracted. An example WSI and ground truth have been shown in Figures 4 (a) and (b). The MS U-Net model was trained for sinus as well as GC regions, while a U-Net was trained for sinus regions.

In the second experiment, in addition to the clean 20 WSIs used before for training, we use 22 more WSIs with noisy or inaccurate annotations. Four additional WSIs with noisy annotations were used for validation.

## 4 Results

### 4.1 U-Net and MS U-Net Compared

The results for U-Net and MS U-Net model are shown below in Table 1 for different test images. The training was performed using Adam optimizer, using constant learning rate of  $10^{-3}$ .

As seen from the IoU scores, the MS U-Net model outperforms the plain U-Net model based on the same training method. This shows the ability of MS U-Net model to better capture the multi-resolution information needed for the segmentation of sinus regions.

Since the germinal centers (GC) are easy to spot compared to the variations observed in a sinus region, the scores for GC region are higher compared to that of sinus regions.

To also do a quality analysis of model predictions, in Figure 4 we have shown one of the testing WSIs, its target mask region indicating the sinus regions, and two images in (c) and (d) which shows the overlap of the model prediction with the ground truth mask, overlayed on the input image. The U-Net model overlay results are shown in (c) and MS U-Net model overlay results in (d). The green region represents sinus area both in the model prediction as well as in target mask (true positives), red region represents model predictions not present

in target mask (false positives), and blue region represents target mask sinus regions not predicted by model (false negatives).

As seen U-Net model results contain much more false positives than MS U-Net model, which is even shown by the difference in their mIoU scores.

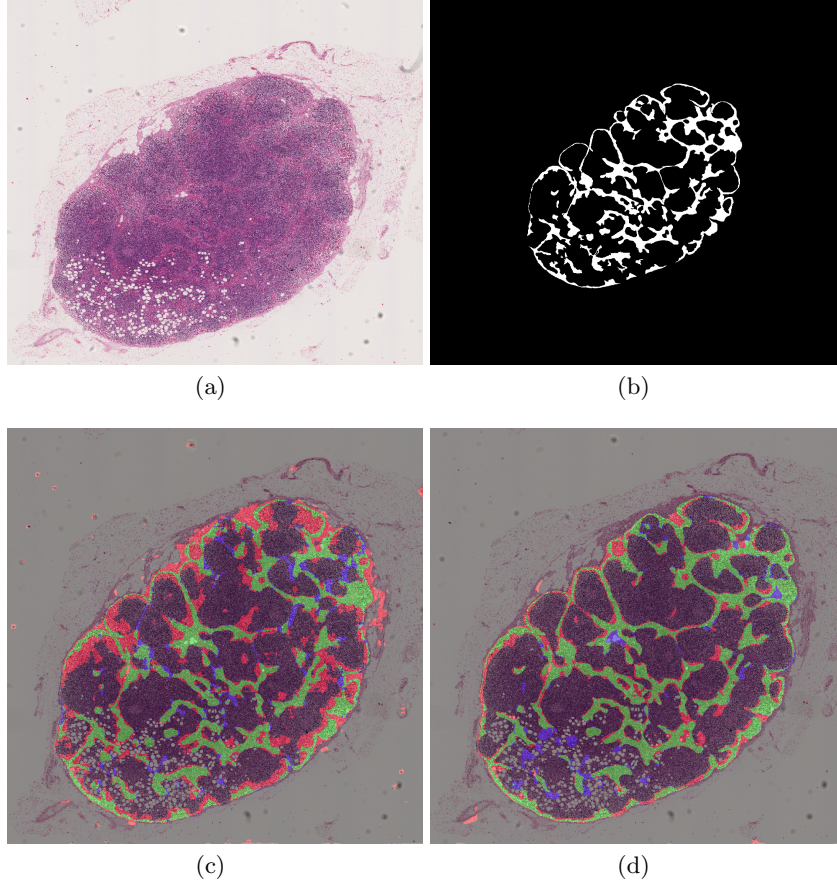


**Fig. 4.** (a) Input WSI of Lymph Node, (b) Target mask to segment Sinus regions from Lymph Node, (c) U-Net model prediction overlay with mask and image, (d) MS U-Net model prediction overlay with mask and image, where green colour represents true positive, blue colour represents false negatives, red colour represents false positives

#### 4.2 MS U-Net with Noise Robust Training

In this subsection, we share the results obtained by including noisy dataset in the training phase, and methods to deal with it.

The MS U-Net sinus prediction results obtained are compared using three different schemes, as shown in Table 2 – one by introducing the fuzzy boundary loss to the MS U-Net model, another by introducing the bootstrapping method,

**Table 1.** Comparison of IoU score of Sinus and Germinal centre IoU scores between different architectures.

WSI Identifier	U-Net MS U-Net		U-Net MS U-Net	
	Sinus	Sinus	GC	GC
Test WSI 1	0.1643	<b>0.4856</b>	0.6123	<b>0.8027</b>
Test WSI 2	0.2836	<b>0.6710</b>	0.4212	<b>0.6844</b>
Test WSI 3	0.2222	<b>0.5876</b>	0.7999	<b>0.9998</b>
Test WSI 4	0.3344	<b>0.5580</b>	0.4333	<b>0.6046</b>
Test WSI 5	0.4500	<b>0.6330</b>	0.4812	<b>0.6605</b>
Average	0.2909	<b>0.5870</b>	0.5496	<b>0.7507</b>

and lastly by combining the fuzzy boundary loss and bootstrapping method. As it can be seen that the performance obtained using both the fuzzy boundaries and bootstrapping method gives the best results.

**Table 2.** Comparing the quantitative improvements of IoU score with Fuzzy Boundaries and Bootstrapping

WSI Identifier	MS-U-Net	MS U-Net	MS U-Net	MS U-Net
		Fuzzy Boundary	Bootstrapping	Fuzzy Boundary + Bootstrapping
Test WSI 1	0.4856	0.5412	0.5600	<b>0.6000</b>
Test WSI 2	0.6710	0.7000	0.7111	<b>0.7333</b>
Test WSI 3	0.5876	0.6010	0.5999	<b>0.6222</b>
Test WSI 4	0.5580	0.5800	<b>0.5333</b>	<b>0.5333</b>
Test WSI 5	0.6330	0.6110	0.6222	<b>0.6400</b>
Average	0.58703	0.6066	0.6053	<b>0.6258</b>

## 5 Conclusion

Our experiments establish the advantage of modifying the U-Net models to include stronger capabilities to handle multiple resolutions. We proposed a simple and effective method modification that employs kernels with different strides and fuses their feature maps to segment histopathology slides with features at various scales. We further analyzed and offered a practical solution that is robust to noisy annotations – those with inexact boundaries and missing annotations. We relaxed the emphasis of cross-entropy loss at the boundaries through Gaussian blurred confidence maps and an auxiliary mask created using bootstrapping a model prediction’s predictions after training it for a few epochs. We compared and contrasted the improvements of each of these methods when the ground truth data is inherently noisy to show that their combination gives the best results, indicating each of these have a role to play in medical image segmentation.

## References

1. John KC Chan. The wonderful colors of the hematoxylin–eosin stain in diagnostic surgical pathology. *International journal of surgical pathology*, 22(1):12–32, 2014.
2. Nikhil Cherian Kurian, Amit Sethi, Anil Reddy Konduru, Abhishek Mahajan, and Swapnil Ulhas Rane. A 2021 update on cancer image analytics with deep learning. *Wiley Interdisciplinary Reviews: Data Mining and Knowledge Discovery*, 11(4):e1410, 2021.
3. Chandradeep Bhatt, Indrajeet Kumar, V Vijayakumar, Kamred Udham Singh, and Abhishek Kumar. The state of the art of deep learning models in medical science and their challenges. *Multimedia Systems*, 27(4):599–613, 2021.
4. Olaf Ronneberger, Philipp Fischer, and Thomas Brox. U-net: Convolutional networks for biomedical image segmentation. In *International Conference on Medical image computing and computer-assisted intervention*, pages 234–241. Springer, 2015.
5. Nabil Ibtehaz and M Sohel Rahman. Multiresunet: Rethinking the u-net architecture for multimodal biomedical image segmentation. *Neural Networks*, 121:74–87, 2020.
6. Jingdong Yang, Jintu Zhu, Hailing Wang, and Xin Yang. Dilated multiresunet: Dilated multiresidual blocks network based on u-net for biomedical image segmentation. *Biomedical Signal Processing and Control*, 68:102643, 2021.
7. Zhiwu Lu, Zhenyong Fu, Tao Xiang, Peng Han, Liwei Wang, and Xin Gao. Learning from weak and noisy labels for semantic segmentation. *IEEE transactions on pattern analysis and machine intelligence*, 39(3):486–500, 2016.
8. David Joon Ho, Dig VK Yarlagadda, Timothy M D’Alfonso, Matthew G Hanna, Anne Grabenstetter, Peter Ntiamoah, Edi Brogi, Lee K Tan, and Thomas J Fuchs. Deep multi-magnification networks for multi-class breast cancer image segmentation. *Computerized Medical Imaging and Graphics*, 88:101866, 2021.
9. Simindokht Jahangard, Mohammad Hossein Zangooei, and Maysam Shahedi. U-net based architecture for an improved multiresolution segmentation in medical images. *arXiv preprint arXiv:2007.08238*, 2020.
10. Yunhe Gao, Chang Liu, and Liang Zhao. Multi-resolution path cnn with deep supervision for intervertebral disc localization and segmentation. In *International Conference on Medical Image Computing and Computer-Assisted Intervention*, pages 309–317. Springer, 2019.
11. Hiroki Tokunaga, Yuki Teramoto, Akihiko Yoshizawa, and Ryoma Bise. Adaptive weighting multi-field-of-view cnn for semantic segmentation in pathology. In *Proceedings of the IEEE/CVF Conference on Computer Vision and Pattern Recognition*, pages 12597–12606, 2019.
12. Nima Tajbakhsh, Laura Jeyaseelan, Qian Li, Jeffrey N Chiang, Zhihao Wu, and Xiaowei Ding. Embracing imperfect datasets: A review of deep learning solutions for medical image segmentation. *Medical Image Analysis*, 63:101693, 2020.
13. Davood Karimi, Haoran Dou, Simon K Warfield, and Ali Gholipour. Deep learning with noisy labels: Exploring techniques and remedies in medical image analysis. *Medical Image Analysis*, 65:101759, 2020.
14. Shaode Yu, Mingli Chen, Erlei Zhang, Junjie Wu, Hang Yu, Zi Yang, Lin Ma, Xuejun Gu, and Weiguo Lu. Robustness study of noisy annotation in deep learning based medical image segmentation. *Physics in Medicine & Biology*, 65(17):175007, 2020.